PAPER

Simulation of pre-breakdown discharges in high-pressure air. I: The model and its application to corona inception

IOP Publishing Journal of Physics D: Applied Physics

J. Phys. D: Appl. Phys. **52** (2019) 355206 (10pp) https://doi.org/10.1088/1361-6463/ab2849

Simulation of pre-breakdown discharges in high-pressure air. I: The model and its application to corona inception

N G C Ferreira[1,2], D F N Santos[1,2], P G C Almeida[1,2], G V Naidis[3] and M S Benilov[1,2,4]

[1] Departamento de Física, FCEE, Universidade da Madeira, Largo do Município, 9000 Funchal, Portugal
[2] Instituto de Plasmas e Fusão Nuclear, Instituto Superior Técnico, Universidade de Lisboa, 1041 Lisboa, Portugal
[3] Joint Institute for High Temperatures, Russian Academy of Sciences, Moscow 125412, Russia

E-mail: benilov@uma.pt

Received 20 March 2019, revised 13 May 2019
Accepted for publication 10 June 2019
Published 4 July 2019

Abstract

A 'minimal' kinetic model of plasmachemical processes in low-current discharges in high-pressure air is formulated, which takes into account electrons, an effective species of positive ions, and three species of negative ions. The model is implemented as a part of numerical model of low-current quasi-stationary discharges in high-pressure air based on the use of stationary solvers, which offer important advantages in simulations of steady-state discharges compared to standard approaches that rely on time-dependent solvers. The model is validated by comparison of the computed inception voltage of corona discharges with several sets of experimental data on glow coronas. A good agreement with the experiment has been obtained for positive coronas between concentric cylinders in a wide range of pressures and diameters of the cylinders. The sensitivity of the computation results with respect to different factors is illustrated. Inception voltages of negative coronas, computed using the values of the secondary electron emission coefficient of 10^{-4}–10^{-3}, agree well with the experimental data. A simplified kinetic model for corona discharges in air, which does not include conservation equations for negative ion species, has been proposed and validated. Modelling of positive coronas in rod-to-plane electrode configuration has been performed and the computed inception voltage was compared with experimental data.

Keywords: gas discharge modelling, kinetics of ionized air, corona discharge, breakdown of high-pressure air

(Some figures may appear in colour only in the online journal)

1. Introduction

The physics of low-current gas discharges (corona, Townsend, and streamer discharges) in high-pressure gases has been understood reasonably well by now and sophisticated numerical models developed, which can follow discharge development on the subnanosecond scale taking into account dozens of plasma species with hundreds of reactions. On the other hand, such models are too heavy to be routinely used in engineering practice and the hold-off voltage in high-voltage devices is usually estimated by evaluating the Townsend ionization integral. Thus, there is a gap between modern methods of numerical modelling of low-current gas discharges and engineering practice, which it is desirable to reduce.

Time-dependent solvers are virtually universally employed in gas discharge modeling, including popular ready-to-use software, e.g. nonPDPSIM [1] and Plasma module of COMSOL Multiphysics, although exceptions exist, e.g. Plasimo [2]. Such solvers are indispensable, in particular, for modelling of fast breakdown of gas-insulated gaps with very

[4] Author to whom any correspondence should be addressed.

short pulses, where the breakdown process cannot be considered as quasi-stationary at any stage from the beginning to the end. On the other hand, breakdown in 50 Hz electric fields may be preceded by a pre-breakdown discharge that is essentially quasi-stationary. In principle, such quasi-stationary discharges may be simulated by means of time-dependent solvers: an initial state of a discharge is specified and its relaxation over time is followed until a steady state has been attained. An alternative is to use stationary solvers, which solve steady-state equations describing a stationary discharge by means of an iterative process unrelated to time relaxation. Stationary solvers offer important advantages in simulations of steady-state discharges. In particular, they are not subject to the Courant–Friedrichs–Lewy criterion or analogous limitations on the mesh element size and they allow decoupling of physical and numerical stability. The removal of limitations on the mesh element size allows one to speed up simulations, with huge improvement in some cases, and is particularly important for modelling of discharges with strongly varying length scales, e.g. corona discharges, where a variation of the mesh element size by orders of magnitude is indispensable.

Thus, it is advantageous to develop an approach to simulation of low-current discharges with the use of stationary solvers. Another step towards facilitating industrial applications would be to formulate and validate a 'minimal' kinetic model of plasmachemical processes in low-current discharges in high-pressure air, which, while being applicable in a wide range of conditions, would be not too heavy computationally. The aim of this work is to formulate such model, to implement it as a part of numerical model of low-current quasi-stationary discharges in high-pressure air based on the use of stationary solvers, and to validate the developed numerical model by comparison of inception voltage of corona discharges, computed in a wide range of conditions, with experimental data on inception of glow coronas.

Note that the developed numerical model gives the minimum voltage required for discharge inception, corresponding to the condition of reproducibility of the charged species inside the discharge gap. The problems of stability and transitions between the corona modes and the inception of a pulse corona can be treated with the use of the formulated plasmachemical model and a combination of stationary and time-dependent solvers as described in [3]; eigenvalue solvers may be helpful as well.

There is vast literature on the physics of corona discharges and a number of useful theoretical results, including analytical ones, have been obtained under various approximations; one can mention papers [4–10] as examples of theoretical work performed over the last 15 years. (It is interesting to note that in the numerical investigation [9] the electron conservation equation was written in the quasi-stationary approximation, which, jointly with the use of simplifications of the physical model, eliminated the constraint on the time step imposed by the electron drift time and thus allowed the time step to be significantly increased. However, the ion conservation equation included the time-dependent term, hence the constraint imposed by the ion drift time remained.) Therefore, a numerical study of the corona discharges is not the task of this work; the consideration is restricted to a comparison of the inception voltage given by the developed numerical model with available experimental data and to a brief discussion of the sensitivity of the model with respect to different factors (the kinetic scheme used, the photoionization, and the secondary electron emission from the cathode).

The outline of the paper is the following. The 'minimal' model of pre-breakdown discharges in air is formulated and relevant numerical aspects are discussed in section 2. In section 3, results of computation of corona inception voltage in the concentric-cylinders configuration are given and compared with the experiment. The sensitivity of the computation results with respect to different factors is illustrated. A simplified model with local kinetics of negative ions is formulated in section 4. In section 5, results are given on inception voltage of positive coronas in the rod-to-plane electrode configuration. A brief summary is given in section 6.

2. Model and numerics

2.1. Equations and boundary conditions

The model of discharges in air, employed in this work, includes equations of conservation and transport of charged species, written in the drift-diffusion approximation, and the Poisson equation:

$$\nabla \cdot \mathbf{J}_\alpha = S_\alpha (\alpha = e,\ \mathrm{M}^+,\ \mathrm{O}_2^-,\ \mathrm{O}^-,\ \mathrm{O}_3^-). \tag{1}$$

$$\varepsilon_0 \nabla^2 \phi = -e \sum_\alpha Z_\alpha n_\alpha. \tag{2}$$

$$\mathbf{J}_\alpha = -D_\alpha \nabla n_\alpha - Z_\alpha n_\alpha \mu_\alpha \nabla \phi. \tag{3}$$

Here subscript α identifies charged species; n_α, $\mathbf{J}_\alpha$, D_α, μ_α, S_α, and Z_α are, respectively, number density, density of transport flux, diffusion coefficient, mobility, volume rate of production, and charge number of species α; ϕ is the electrostatic potential; e is the elementary charge; and ε_0 is the permittivity of free space. The charged species included in the model are the electrons, an effective species of positive ions, designated M^+, where $\mathrm{M} = \mathrm{O}_2$, N_2, and the negative ions O_2^-, O^- and O_3^-.

The source terms S_α in equations for electrons and positive ions include, in addition to terms describing production of these species in collisional processes, the photoionization term S_{ph}. The latter is evaluated by means of the three-exponential Helmholtz model [11] :

$$S_{ph}(\mathbf{r}) = \sum_{j=1}^{3} S_{ph}^{(j)}(\mathbf{r}), \tag{4}$$

with each of the terms satisfying the Helmholtz partial differential equation,

$$\nabla^2 S_{ph}^{(j)}(\mathbf{r}) - (\lambda_j p_{\mathrm{O}_2})^2 S_{ph}^{(j)}(\mathbf{r}) = -A_j p_{\mathrm{O}_2}^2 I(\mathbf{r}) (j = 1, 2, 3). \tag{5}$$

Here A_j and λ_j are constants (parameters of the three-exponential fit function) given in [11], p_{O_2} is the partial pressure of molecular oxygen, and $I(\mathbf{r})$ is the product of ξ the probability

Table 1. Kinetic scheme and relevant kinetic data.

Number	Reaction	Data for evaluation of reaction rate	Reference
1	$e + M \rightarrow 2e + M^+$	[a] Equation (12)	
2	$e + O_2 \rightarrow O^- + O$	[a] Equation (13)	
3	$e + O_2 + M \rightarrow O_2^- + M$	[a] $\frac{\eta_3}{N^2} = 1.6 \times 10^{-47} (E/N)^{-1.1}$ m^5	[15]
4	$M + h\nu \rightarrow e + M^+$	[b] Equations (4)–(6)	[11]
5	$O_2^- + M \rightarrow e + O_2 + M$	[c] $1.24 \times 10^{-17} \exp\left[-\frac{179}{8.8+(E/N)}\right]^2$ m^3 s^{-1}	[16]
6	$O^- + N_2 \rightarrow e + N_2O$	[c] $1.16 \times 10^{-18} \exp\left[-\frac{48.9}{11+(E/N)}\right]^2$ m^3 s^{-1}	[16]
7	$O^- + O_2 \rightarrow O + O_2^-$	[c] $6.96 \times 10^{-17} \exp\left[-\frac{198}{5.6+(E/N)}\right]^2$ m^3 s^{-1}	[16]
8	$O^- + O_2 + M \rightarrow O_3^- + M$	[c] $1.1 \times 10^{-42} \exp\left[-\frac{(E/N)}{65}\right]^2$ m^6 s^{-1}	[16]

Notes: *E/N* in Td, M denotes any of the molecules N_2 and O_2.
[a] Townsend coefficient.
[b] Reaction rate.
[c] Reaction rate constant.

of ionization of a molecule at photon absorption and the local photon production rate. The latter is assumed to be proportional to the rate of ionization of neutral molecules by electron impact, $S_i(\mathbf{r})$, and $I(\mathbf{r})$ is written as

$$I(\mathbf{r}) = \xi \frac{p_q}{p + p_q} \frac{\nu_u}{\nu_1} S_i(\mathbf{r}), \tag{6}$$

where p is the neutral gas pressure, $p_q/(p + p_q)$ is a quenching factor that accounts for the probability of non-radiative de-excitation of nitrogen molecules due to collisions with other molecules, ν_u is the frequency of electron impact excitation of radiating states producing ionizing photons, and ν_1 is the electron impact ionization frequency.

Following [4, 12], the quenching pressure p_q is set equal to 30 Torr and the product $\xi\nu_u/\nu_1$ is expressed in terms of the the reduced electric field *E/N* (here $E = |\nabla\phi|$ and N is the number density of neutral molecules):

$$\xi \frac{\nu_u}{\nu_1} = 0.03 + \frac{15.7\,\text{Td}}{E/N}. \tag{7}$$

Boundary conditions are written in the conventional form. At the cathode, the electrons are emitted from the surface with the effective secondary emission coefficient γ being varied in the modelling between 0 and 10^{-2}; the diffusion flux of the attracted particles (the positive ions) is neglected in comparison with the drift flux; the negative ions are repelled by the electric field and thus their number density is defined by the chaotic flux; the electrostatic potential is set equal to zero; the rate of photoionization is set to zero:

$$(J_e)_n = -\gamma (J_{M^+})_n, \quad \frac{\partial n_{M^+}}{\partial n} = 0,$$
$$(J_\alpha)_n = \frac{n_\alpha}{2} \sqrt{\frac{8kT_-}{\pi m_\alpha}} (\alpha = O_2^-,\ O^-,\ O_3^-), \tag{8}$$

$$\phi = 0, \quad S_{ph}^{(j)} = 0. \tag{9}$$

Here and further k is Boltzmann's constant, m_α is the mass of species α, T_- and T_+ are temperatures of negative and positive ions, respectively, and n is a direction locally orthogonal to the boundary of the computation domain (the cathode surface, in this case) and directed outward of the domain.

At the anode, the diffusion flux of the attracted particles (the electrons and the negative ions) is neglected in comparison with the drift flux; the positive ions are repelled by the electric field and thus their number density is defined by the chaotic flux; the electrostatic potential is fixed at some value U; the rate of photoionization is set to zero:

$$\frac{\partial n_\alpha}{\partial n} = 0 (\alpha = e,\ O_2^-,\ O^-,\ O_3^-),$$
$$(J_{M^+})_n = \frac{n_{M^+}}{2} \sqrt{\frac{8kT_+}{\pi m_{M^+}}}, \quad \phi = U, \quad S_{ph}^{(j)} = 0. \tag{10}$$

Results reported in this work refer to two corona discharge configurations: a one-dimensional corona between concentric cylinders and a two-dimensional corona in the rod-to-plane gaps. Boundary conditions at the boundaries limiting the computation domain need to be specified for the rod-to-plane configuration: the so-called natural boundary conditions (zero normal derivatives) for all dependent variables (n_α, ϕ, $S_{ph}^{(j)}$) were used.

2.2. Transport coefficients and kinetics

The local-field approximation is employed, i.e. the electron transport and kinetic coefficients are assumed to be dependent on the local reduced electric field *E/N* only.

The mobility of the positive ions was set equal to the mobility of N_2^+ in N_2 and computed by means of the code [13], which realizes the model [14]. The mobility of the electrons was taken from [15] and the mobilities of the negative ions O_2^-, O^-, and O_3^- were taken from [16]. The diffusion coefficients of all ion species are related to the mobilities through Einstein's relation with the corresponding temperature T_+ or T_-. The longitudinal and transversal electron diffusion coefficients were evaluated with the use of the online version of the

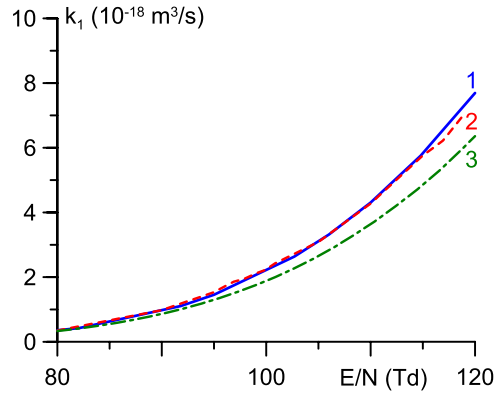

Figure 1. Ionization rate constant. 1: evaluation with the use of equation (12). 2: experimental data for air from figure 5(b) of [20]. 3: evaluation with the use of the online version of the Bolsig+ solver [17] and the cross sections [18].

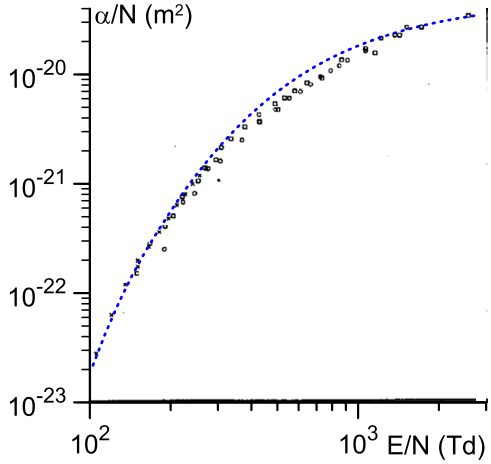

Figure 2. Townsend ionization coefficient. Dotted: equation (12). Points: data from figure 4.4 of [19].

Bolsig+ solver [17] and the cross sections [18]. Temperature T of neutral gas is assumed to be constant; results reported in this work refer to $T = 300$ K. T_+ was computed by means of the code [13] and T_- was set equal to 300 K.

The kinetic scheme for air assumed in this work is shown in table 1 and comprises the following processes: electron impact ionization (reaction 1), two-body (dissociative) attachment (2), three-body attachment (3), photoionization (4), collisional detachment from O_2^- (5), associative detachment from O^- (6), charge transfer from O^- to O_2^- (7), and conversion of O^- to O_3^- (8). Note that the test simulations, performed with account of recombination of electrons with positive ions and ion-ion recombination, have shown that the recombination processes are negligible in the whole range of conditions considered; an expected result stemming from low charged particle densities characteristic of pre-breakdown discharges. Therefore, the recombination processes are not taken into account in the simulations reported in this work (and, accordingly, are not included in table 1).

The rates of electron impact ionization, reaction 1, and two- and three-body attachment, reactions 2 and 3, are evaluated in terms of the Townsend coefficients, which are related

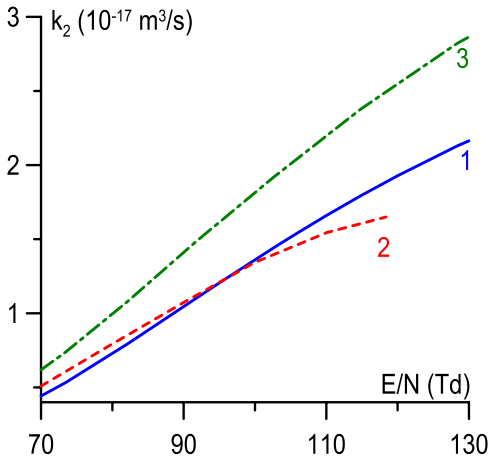

Figure 3. Dissociative attachment rate constant. 1: evaluation with the use of equation (13). 2: experimental data for an N_2–O_2 mixture with 20% oxygen from figure 6(b) of [20], recalculated to the rate constant. 3: evaluation with the use of the online version of the Bolsig+ solver [17] and the cross sections [18].

to the corresponding reaction rate constants k_i by the conventional formulas

$$\alpha = \frac{k_1 N}{\mu_e E}, \eta_2 = \frac{k_2 n_{O_2}}{\mu_e E}, \eta_3 = \frac{k_3 n_{O_2} N}{\mu_e E}. \tag{11}$$

The Townsend ionization coefficient is evaluated by means of an expression approximating the experimental data compiled in [19] and the new experimental data [20]:

$$\frac{\alpha}{N} = \begin{cases} 1.64 \times 10^{-20} \exp\left[-\frac{680}{(E/N)}\right] \text{ m}^2, & \text{if} \quad E/N < 186 \text{ Td}, \\ \left[1 + \frac{6\times10^6}{(E/N)^3}\right] 5 \times 10^{-20} \exp\left[-\frac{1010}{(E/N)}\right] \text{ m}^2, & \text{if} \quad E/N > 186 \text{ Td}. \end{cases} \tag{12}$$

In figures 1 and 2 the ionization rate constant and the Townsend ionization coefficient in air determined with the use of equation (12) are shown along with the experimental data from [20] and [19], respectively. Also shown in figure 1 is the ionization rate constant determined with the use of the online version of the Bolsig+ solver [17] and the cross sections [18]. Note that a detailed discussion of the ionization rate constant for air at low reduced electric fields can be found in [21].

The Townsend coefficient of the two-body (dissociative) attachment, reaction 2 of table 1, is taken as

$$\frac{\eta_2}{N} = 3.44 \times 10^{-23} \exp\left[-1.05\,|5.3 - \ln(E/N)|^3\right] \text{ m}^2. \tag{13}$$

This formula represents a modification of an expression that can be obtained from the expression for the rate constant given in [22], reaction 20 in table A1 of [22]. (The factor of 0.8 was introduced to fit new experimental data [20]. The vibrational temperature in typical conditions of corona discharge does not significantly exceed the translational temperature, therefore the factor F in the expression [22], which accounts for gains in electron energy in collisions with vibrationally excited nitrogen molecules, or, in other words, for the effect of non-zero vibrational temperature, was dropped.)

In figure 3 the rate constant of dissociative attachment, computed using equation (13), is shown along with new experimental data [20]. Also shown in figure 3 are values determined

with the use of the online version of the Bolsig+ solver [17] and the cross sections [18]. It is seen that the approximation (13) is in reasonable agreement with the data [20], however one should keep in mind that the available experimental data have a significant scatter; e.g. figure 6 of [21].

The rate of photoionization, reaction 4 of table 1, is evaluated by means of equations (4)–(6) as described in section 2.1. Expressions used for rate constants of all the other reactions are given in the table 1.

The above kinetics refer to dry air. In the experiments, ambient air is typically used (usually with non-controlled humidity), containing water vapor at a molar fraction of around 1%. A correction of parameters of the model (kinetic coefficients, photoionization efficiency, etc) is required for simulations of discharges in humid air. Available data on the ionization and attachment coefficients [23, 24] and on photoionization [25] show that admixture of small amount of water vapor, of around one percent, does not change substantially the values of these parameters. Results of simulations of positive coronas in humid air [26, 27] accounting the effects mentioned above show that the variation of corona inception voltage with humidity does not exceed about 5%. On the other hand, experiments with controlled humidity [26, 28–30] also show that the corona inception voltage changes with humidity nearly in the same range. Considering the above and the fact that the objective of this work is to formulate a 'minimal' model, the inclusion of humidity effects is at this stage hardly advisable.

2.3. Numerical aspects

The above-stated problem was solved numerically by means of stationary solvers, which, as already discussed in the Introduction, offer important advantages in simulations of quasi-stationary discharges compared to time-dependent solvers. Another important feature of the modelling was switching between discharge voltage U and discharge current I as the control parameter.

A delicate point in using stationary solvers is finding a suitable initial approximation. In this work, numerical simulation of each electrode configuration was started in the following way. A term of the order of 10^{16} m^{-3} s^{-1} or smaller, describing an artificial external ionization source, is added to equation (1) for the electrons and the positive ions. The effect of this term is the existence of a non-trivial solution (i.e. a solution with non-zero densities of the charged particles) for applied voltages U below the corona inception voltage U_c. A steady-state solution is found for an applied voltage U that is supposed to be below U_c and the corresponding value I_0 of the discharge current is computed. After this, the control parameter is switched to the discharge current, which is fixed at $I = I_0$. The external ionization source term is then reduced in small steps and the solution is recomputed at each step (note that values of the discharge voltage, computed at each step, gradually increase), until this term has been completely removed from the equations. Thus the first steady-state solution, which describes the corona discharge for $I = I_0$, is obtained. The corresponding discharge voltage represents the inception voltage U_c. This solution can be used as the initial approximation for any subsequent simulations in which parameters of interest (e.g. the discharge current or plasma pressure) are varied.

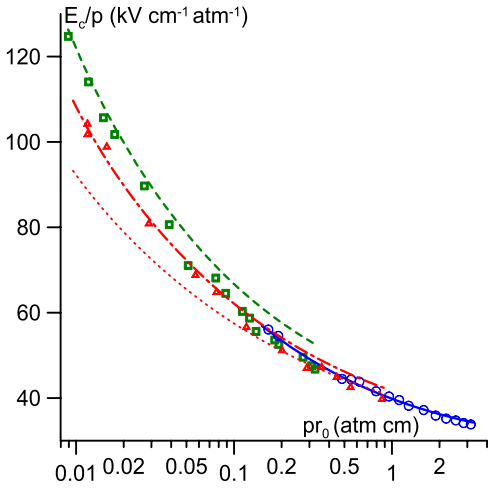

Figure 4. Reduced inception field at the surface of positive wire electrode. Circles and solid line: experimental data [33] and the corresponding modelling, $p = 1$ atm, $2R = 58.1$ cm, varying inner cylinder diameter $2r_0$. Triangles and dash-dotted line: experimental data [32] and the corresponding modelling, $2r_0 = 0.239$ cm, $2R = 9.75$ cm, varying pressure. Squares and dashed line: experimental data [32] and the corresponding modelling, $2r_0 = 0.0178$ cm, $2R = 9.75$ cm, varying pressure. Dotted line: modelling with the normal derivative of the rate of photoionization set to zero at the electrodes, $2r_0 = 0.239$ cm, $2R = 9.75$ cm, varying pressure.

The simulations have been performed with the use of commercial software COMSOL Multiphysics. The species conservation equation (1), supplemented with the transport equation (3), were formulated in logarithmic variables, i.e. new dependent variables $N_a = \ln n_\alpha$ have been introduced, and solved with the use of module Transport of Diluted Species. The latter was supplemented with the consistent streamline upwind Petrov–Galerkin weighted residual stabilization. As another stabilization means, artificial source terms C/n_a were added to S_a on the rhs of equation (1). The constant C was scaled to ensure that these terms do not affect the solution, while still ensuring the convergence of the iterations. The module Electrostatics was used to solve the Poisson equation (2).

3. Corona between concentric cylinders

A number of experiments on inception of glow corona in air are reported in the literature; e.g. [26, 31–35]. Typical electrode configurations are concentric cylinders and point-to-plane. Results of computation of inception of corona between concentric cylinders under conditions of experiments [32, 33] are reported in this section. Experimental results on the inception voltage U_c in this geometry are conventionally reported in terms of the corona inception field strength E_c, which is related to the inception voltage as

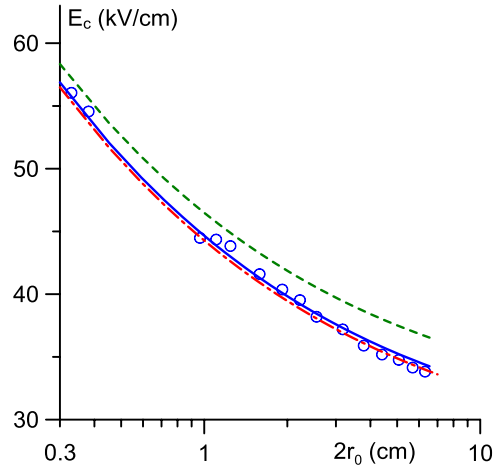

Figure 5. Inception field at the surface of positive wire electrode in atmospheric-pressure air. $2R = 58.1$ cm, varying inner cylinder diameter $2r_0$. Lines: computations with various kinetic schemes. Solid: kinetic scheme of table 1. Dashed: kinetic scheme without account of detachment process. Dash-dotted: kinetic scheme of table 1 with rates of attachment (reactions 2 and 3) set to zero. Circles: experimental data [33].

$$E_c = \frac{U_c}{r_0 \ln(R/r_0)}, \tag{14}$$

where r_0 and R are the radii of the inner and outer cylinders, respectively. The same relation is used in order to determine the inception field in the modelling. The discharge current I was set equal to 1 nA per centimeter of the cylinder length, which is sufficiently small for the discharge voltage computed to be independent of I and thus to be considered as the corona inception voltage U_c. The effective secondary electron emission coefficient γ was set equal to zero unless specified otherwise.

In the case of positive corona, where the smaller electrode (the inner cylinder) plays the role of anode and the larger electrode (the outer cylinder) is a cathode, the discharge is generally stable and the reproducibility of experimental data is better than for negative coronas. Therefore, positive glow coronas are more suitable for validation of quasi-stationary theoretical models.

In figure 4, values of the reduced inception field of a positive corona computed in a wide range of conditions are plotted as a function of pr_0 along with experimental data [32, 33]. The agreement between computed and measured inception field is quite good, except for a small deviation between the dashed line and squares appearing in the range $pr_0 \gtrsim 0.1$ atm cm (which corresponds to the pressure range from 10 to 35 atm).

There is a visible difference in figure 4 in the range $pr_0 < 0.1$ atm cm between the experimental data [32] for the same pr_0 referring to the two different r_0 values. This effect is caused by a decrease of photoionization rate with growth of pressure, originating in collisional quenching of nitrogen radiating states (a detailed discussion of this topic is given in [4]). Let us consider an illustrative example. At $pr_0 = 0.03$ cm atm, the gas pressure and the value of E_c/p are 3.37 atm and 88.93 kV cm^{-1} atm^{-1} for $2r_0 = 0.0178$ cm and 0.25 atm and 81.01 kV cm^{-1} atm^{-1} for $2r_0 = 0.239$ cm. The value of E_c/p for $2r_0 = 0.0178$ cm was recomputed with the pressure equal to 3.37 atm except in the evaluation of S_{ph}, where it was set equal to 0.25 atm. The obtained E_c/p value was 83.23 kV cm^{-1} atm^{-1}, which is much closer to the above-cited value of 81.01 kV cm^{-1} atm^{-1}. Thus, the effect of pressure on the reduced inception field (at given pr_0), observed in the experiments, could hardly be explained without photoionization.

Modelling was performed also for the case where the boundary condition $S_{ph}^{(j)} = 0$ for the rate of photoionization at the inner cylinder or at both electrodes was replaced with the zero-derivative condition $\partial S_{ph}^{(j)}/\partial n = 0$, which amounts to neglecting losses of photons to the inner cylinder or both electrodes. The results of the two sets of modelling were quite close, meaning that the loss of photons on the outer electrode is a minor effect, which, of course, could be expected. These results are depicted in figure 4 by the dotted line. One can see that values of the inception field are sensitive to the choice of the boundary condition for photoionization at the anode for low pressures. For higher values of pressure, the effect of the boundary condition for photoionization at the anode is attenuated.

In figure 5, the experimental data [33] and the corresponding modelling results, which are shown in figure 4 by the open circles and the solid line, are replotted as functions of the diameter of the anode $2r_0$. The dashed line corresponds to E_c computed without account of detachment (reactions 5 and 6 in table 1). The dash-dotted line in figure 5 depicts computations without account of attachment (reactions 2 and 3). One can see that the disregard of detachment results in an increase of the inception voltage as it should. On the other hand, the dash-dotted line, computed without account of both attachment and detachment, is close to the solid one, which suggests that the detachment approximately compensates the attachment.

The above results refer to the secondary electron emission coefficient γ equal to zero. A relevant question is how sensitive the results are with respect to the value of γ. In figure 6, the reduced inception field computed with different values of γ for conditions of the experiment [32] is shown along with the experimental data. Note that the line corresponding to $\gamma = 0$ would coincide, to the graphical accuracy, with the (solid) line corresponding to $\gamma = 10^{-6}$ and therefore is not shown on the graph. As expected, the reduced inception field decreases with increase of γ. Good agreement with the experiments is seen for γ not exceeding 10^{-4}. Note that real values of γ in air seem to be of this order of magnitude for low E/p values at the cathode surface [36].

Also shown in figure 6 are simulations performed for $\gamma = 10^{-6}$ without account of photoionization. As expected, the disregard of photoionization causes an increase of the reduced inception field. The effect is stronger for low values of pr_0; for the same value of pr_0, the effect is stronger for lower pressures (figure 6(a)). There is an appreciable deviation of the inception field computed without account of photoionization from the experimental data.

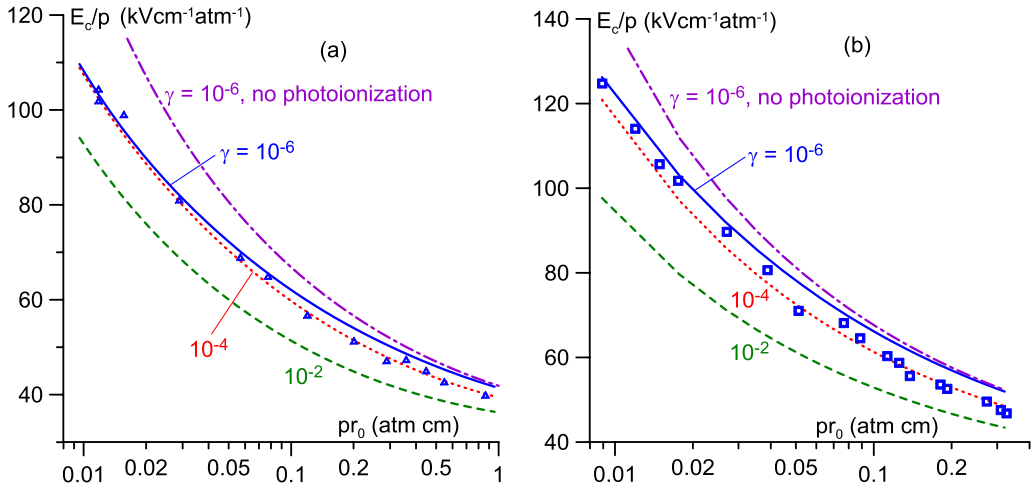

Figure 6. Reduced inception field at the surface of positive wire electrode. $2R = 9.75$ cm, varying pressure. Lines: modelling with different values of the secondary electron emission coefficient γ. Dash-dotted: modelling with $\gamma = 10^{-6}$ without account of photoionization. Points: experimental data [32]. (a) $2r_0 = 0.239$ cm. (b) $2r_0 = 0.0178$ cm.

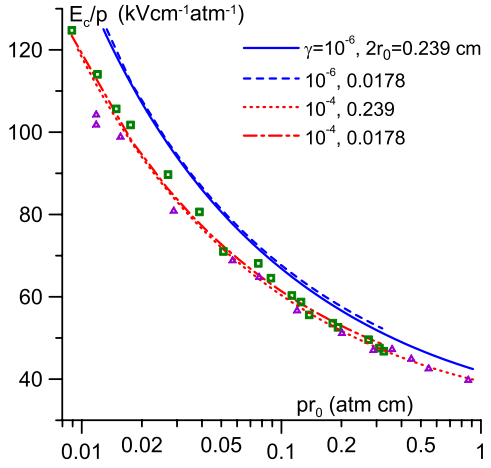

Figure 7. Reduced inception field at the surface of positive wire electrode. $2R = 9.75$ cm, varying pressure. Lines: modelling without account of photoionization with different values of the secondary electron emission coefficient γ and wire diameter $2r_0$. Points: experimental data [32] for $2r_0 = 0.239$ cm (triangles) and $2r_0 = 0.0178$ cm (squares).

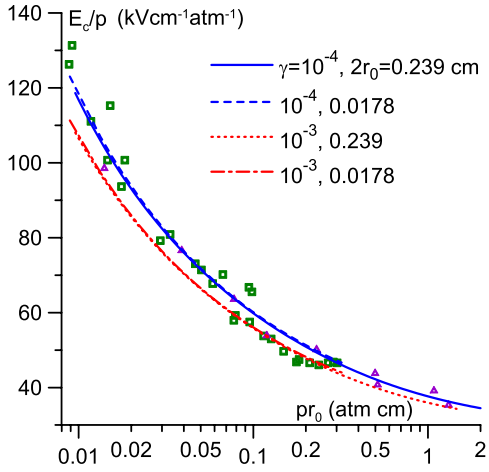

Figure 8. Reduced inception field at the surface of negative wire electrode. $2R = 9.75$ cm, varying pressure. Lines: modelling with different values of the secondary electron emission coefficient γ and wire diameter $2r_0$. Points: experimental data [32] for $2r_0 = 0.239$ cm (triangles) and $2r_0 = 0.0178$ (squares).

The reduced inception field, computed without account of photoionization for two values of the secondary electron emission coefficient, $\gamma = 10^{-4}$ and 10^{-6}, is shown in figure 7. One can see that the effect of secondary electron emission turns more pronounced if the photoionization is neglected, as it should. For $\gamma = 10^{-4}$, the deviation of the computed inception field from the experimental data is not very large. On the other hand, the reduced electric field, computed as a function of pr_0 without account of photoionization, does not reveal a dependence on pressure for both $\gamma = 10^{-6}$ and $\gamma = 10^{-4}$ (the solid and dashed lines in figure 7 are quite close, as well as the dotted and dash-dotted ones). One can conclude once again that the effect of pressure on the reduced inception field (at a given pr_0 value), observed in the experiments, could hardly be explained without photoionization.

The above results refer to positive coronas. In the case of negative coronas, a steady-state regime does not usually occur and current pulses are superposed on a DC current component, although the pulse component decreases with increasing voltage. Due to high electric fields at the surface of the smaller electrode, values of the secondary electron emission coefficient appropriate for negative coronas are higher than those for positive coronas and the secondary electron emission is likely to play a role. Hence, characteristics of negative corona depend on the cathode material, through the secondary electron emission coefficient, and on the state of the cathode surface. There is also a problem of identification of corona inception voltage in the experiment; e.g. [32]. Therefore, negative coronas are not suitable for validation of quasi-stationary models of corona discharges. On the other hand, the scatter of experimental data may be reduced by means of appropriate filtering, and it would be of interest to compare such filtered data with computation results.

In figure 8, experimental data on negative corona inception field, reported in [32], are shown. Note that in the experiments

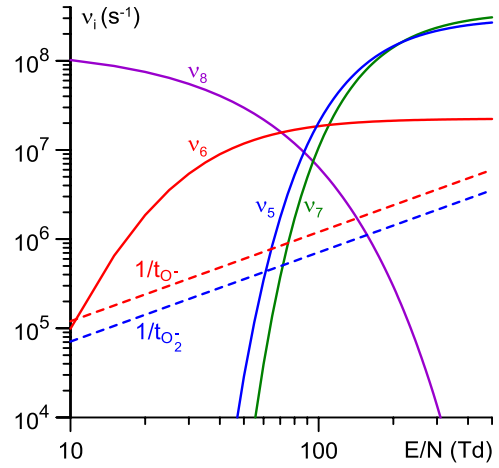

Figure 9. Frequencies of ion-molecular reactions and the inverse of the characteristic times of drift of the ions O_2^- and O^- as functions of the reduced electric field, $p = 1$ atm.

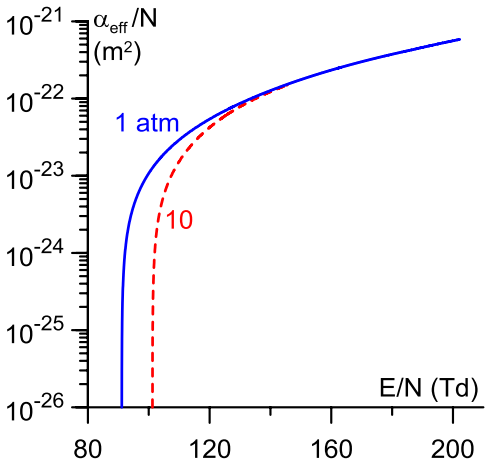

Figure 10. Effective ionization coefficient.

[32] the corona electrodes with the diameters of 0.0178 cm and 0.239 cm were made of tungsten and stainless steel, respectively. Also shown is the inception field computed using two values of the secondary electron emission coefficient γ, taken in agreement with [37]. One can see that the computed reduced negative corona inception field, considered as a function of pr_0, does not reveal a visible dependence on r_0 (or, equivalently, pressure), in agreement with the experiment. This contrasts the case of positive coronas, treated above, and is a consequence of the role of photoionization being minor for negative coronas. The same set of γ values, independent of pressure, allows one to evaluate the negative corona inception field, for both electrode radii and materials, in agreement with the experiment.

4. Model with local kinetics of negative ions

In figure 9, frequencies of ion-molecule reactions, reactions 5–8 in table 1, are shown as functions of the reduced electric field. The frequencies are defined in the usual way, $\nu_5 = k_5 N$, $\nu_6 = k_6 n_{N_2}$, $\nu_7 = k_7 n_{O_2}$, $\nu_8 = k_8 n_{O_2} N$. The data shown in the figure refer to the plasma pressure $p = 1$ atm; for other pressures the frequencies ν_5 to ν_7 will be scaled proportionally to p and ν_8 proportionally to p^2. Note that the critical reduced electric field in the framework of the kinetic model considered is around 100 Td.

Let us consider also characteristic times of drift of the ions O_2^- and O^-: $t_i = l/\mu_i E$, where $i = O^-$, O_2^- and l is a local characteristic length scale. Under conditions considered, l is of the order of 100 μm to 1 mm in the active zone and of 1 cm to 10 cm in the drift zone. The inverse of the characteristic times for $l = 1$ mm are shown in figure 9.

The ions O^- are produced in reaction 2 and destroyed in reactions 6–8. One can see from figure 9 that the sum of frequencies of these reactions, $\nu_6 + \nu_7 + \nu_8$, significantly exceeds $1/t_{O^-}$. Hence, the lhs of the equation of conservation, equation (1), of the ions O^- may be neglected and this equation to the first approximation assumes the form of the equation of local balance

$$\nu_2 n_e = (\nu_6 + \nu_7 + \nu_8)\, n_{O^-}. \tag{15}$$

The ions O_2^- are produced in reactions 3 and 7 and destroyed in reaction 5. One can see that the inequality $\nu_5 \gg 1/t_{O_2^-}$ holds in the active zone and in the adjacent section of the drift zone. In this domain, the equation of conservation of ions O_2^- to the first approximation assumes the form of the equation of local balance

$$\nu_3 n_e + \nu_7 n_{O^-} = \nu_5 n_{O2^-}. \tag{16}$$

Using relations (15) and (16), one can show that

$$\nu_2 n_e + \nu_3 n_e - \nu_5 n_{O_2^-} - \nu_6 n_{O^-} = \frac{\nu_2 \nu_8}{\nu_6 + \nu_7 + \nu_8} n_e. \tag{17}$$

The quantity on the rhs of this relation has the meaning of the effective attachment rate, which accounts for dissociative and three-body attachment, collisional detachment from O_2^-, associative detachment from O^-, charge transfer from O^- to O_2^-, and conversion of O^- to O_3^-. One can introduce also the effective ionization coefficient

$$\alpha_{\text{eff}} = \alpha - \eta_2 \frac{\nu_8}{\nu_6 + \nu_7 + \nu_8}. \tag{18}$$

The effective ionization coefficient defined by equation (18) is shown in figure 10 as a function of reduced field for two values of the plasma pressure $p = 1$ atm and 10 atm. The critical reduced field, at which the effective ionization coefficient vanishes, equals 91 Td for $p = 1$ atm and 101 Td for $p = 10$ atm and increases with pressure. The reason for the latter is an increase in conversion of O^- ions to stable ions O_3^- at higher pressures. Note that values of critical reduced field obtained in [16] are 93 Td for $p = 1$ atm and 109 Td for $p = 10$ atm. While the former value is close to the above-cited value obtained in this work, the difference in the values for $p = 10$ atm is more appreciable.

Thus, we have obtained a simplified model, which does not include equations of conservation of negative ion species and accounts for attachment and ion-molecular reactions by means of the effective attachment rate in the conservation equation for electrons: the model with local kinetics of negative ions. Simulations for the whole range of conditions of

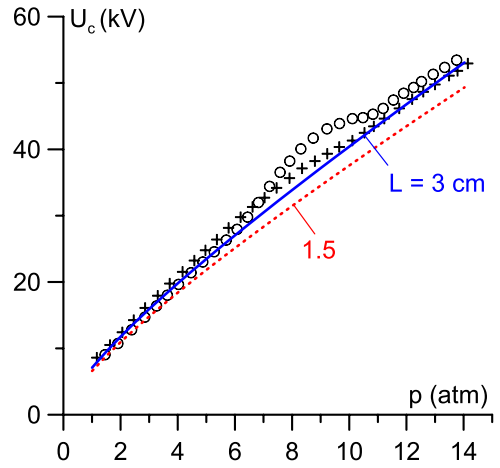

Figure 11. Positive corona inception voltage in rod-to-plane configuration. Hemispherically-tipped rod, diameter of 0.094 cm, 1 cm gap, plate diameter of 3.49 cm. Lines: modelling with different values of the rod length L. Points: experimental data [31] (two separate series of experiments).

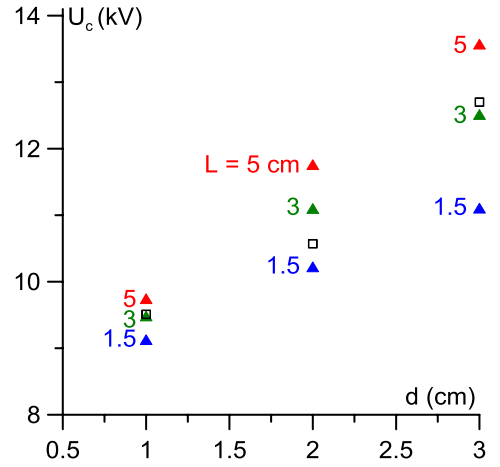

Figure 12. Positive corona inception voltage in rod-to-plane configuration. d: the gap length. Hemispherically-tipped rod, diameter of 2 cm, plate diameter of 7 cm, $p = 1$ atm. Triangles: modelling with different values of the rod length L. Squares: experimental data [35].

experiments [32, 33], performed with the use of this model and with the use of the full model (including the conservation equations for all negative ion species), gave values of the inception field that are very close to each other (within 1% or so). This attests to the possibility of modelling discharge inception using the model with local kinetics of negative ions, with advantages in terms of computational costs.

In principle, the model with local kinetics of negative ions may be used also for evaluation of the ionization integral $K = \int \alpha_{\text{eff}}\, dr$ (the integration is extended over the active zone). As an example, we note that the ionization integral, evaluated for the inception voltage of positive corona under conditions of the experiment [32] with $2r_0 = 0.239$ cm, varies from 6.7 for $p = 0.08$ atm to 12.8 for $p = 17$ atm; values that agree well with estimates [4]. The ionization integral at inception of negative corona varies much less; for example, for $\gamma = 10^{-4}$ and $2r_0 = 0.239$ cm it equals 8.7 for $p = 0.08$ atm and 8.1 for $p = 17$ atm. These values are not very different from $\ln\left(1 + \gamma^{-1}\right) \approx 9.2$, as could be expected. (Note that the difference can be due to ion currents being non-negligible at the edge of the active zone.)

5. Positive corona in rod-to-plane configuration

The computed inception voltages of the positive corona in the rod-to-plane configuration in air under the conditions of the experiments [31, 35] are shown in figures 11 and 12. (The simulations have been performed for the discharge current $I = 1$ nA.)

The parameters of the experimental geometry, reported in [31, 35], are the rod and plate (cathode) diameters and the rod-to-plane distance (length of the discharge gap); the rod length is omitted. The latter is a typical situation: there seems to be no experimental publications where the rod length would be indicated.

For this reason, the modelling results shown in figures 11 and 12 refer to different values of the rod length L. These results show that, while the effect of the rod length on the inception voltage is not very strong, it is still quite appreciable, especially for large discharge gaps. Good agreement with the experimental data reported in [31, 35] is obtained for $L = 3$ cm.

6. Summary

Modern numerical models of low-current high-pressure gas discharges, which take into account dozens of plasma species with hundreds of reactions and can follow discharge development on the subnanosecond scale, are too heavy to be routinely used in engineering practice and the hold-off voltage in high-voltage devices is usually estimated by evaluating the Townsend ionization integral. With the aim to reduce this gap, a 'minimal' kinetic model of plasmachemical processes in low-current discharges in high-pressure air is formulated. The kinetic scheme takes into account electrons, an effective species of positive ions, and negative ions O_2^-, O^-, and O_3^-. Relevant kinetic and transport coefficients are given. The model is implemented as a part of a numerical model of low-current quasi-stationary discharges in high-pressure air based on the use of stationary solvers, which offer important advantages in simulations of quasi-stationary discharges.

The numerical model developed is validated by a comparison of inception voltage of glow corona discharges, computed in a wide range of conditions, with several sets of experimental data. A good agreement with experimental data has been obtained for positive coronas between concentric cylinders in a wide range of pressures and diameters of the cylinders, which attests to the suitability of the kinetics employed. The sensitivity of the computation results with respect to different factors is illustrated: the kinetic scheme used; the photoionization and a boundary condition for the photoionization rate at solid surfaces; the secondary emission from the cathode. It is shown, in particular, that the effect of pressure on the reduced

inception field (at given pr_0), observed in the experiments, could hardly be explained without photoionization.

Computed inception voltages of negative coronas depend on the value of the secondary electron emission coefficient γ, assumed in the modelling. The voltage computed with γ of 10^{-4}–10^{-3} agrees well with the experimental data.

A simplified kinetic model for corona discharges has been proposed and validated. The model does not include conservation equations for negative ion species and accounts for ion-molecular reactions by means of the effective attachment rate in the conservation equation for electrons. The ionization integral evaluated with the use of this model at corona inception voltage varies significantly for positive coronas; in the case of negative coronas, the ionization integral varies much less and is not very different from $\ln\left(1+\gamma^{-1}\right)$, as could be expected.

The computed inception voltage of positive glow coronas in the rod-to-plane electrode configuration qualitatively agrees with experimental data. The modelling results show that the inception voltage is affected by the rod length, a parameter omitted in experimental papers. A good quantitative agreement with the experiment can be obtained by variation of the rod length in the modelling.

Acknowledgments

The work at Universidade da Madeira was supported by the project UID/FIS/50010/2019 of FCT—Fundação para a Ciência e a Tecnologia of Portugal and by the project PlasMa—M1420-01-0145-FEDER-000016, co-financed by the Operational Program of the Autonomous Region of Madeira 2014–2020.

ORCID iDs

N G C Ferreira https://orcid.org/0000-0001-5938-4182
D F N Santos https://orcid.org/0000-0002-2377-766X
P G C Almeida https://orcid.org/0000-0002-8395-2693
G V Naidis https://orcid.org/0000-0003-2184-802X
M S Benilov https://orcid.org/0000-0001-9059-1948

References

[1] Kushner M J 2005 *J. Phys. D: Appl. Phys.* **38** 1633
[2] van Dijk J, Peerenboom K, Jimenez M, Mihailova D and van der Mullen J 2009 *J. Phys. D: Appl. Phys.* **42** 194012
[3] Ferreira N G C, Almeida P G C, Naidis G V and Benilov M S 2017 *Proc. 23rd ICPIG (Estoril, Portugal, 9–14 July 2017)* p 325
[4] Naidis G V 2005 *J. Phys. D: Appl. Phys.* **38** 2211
[5] Aleksandrov N L, Bazelyan E M, D'Alessandro F and Raizer Y P 2006 *J. Electrost.* **64** 802
[6] Zheng Y, Zhang B and He J 2011 *Phys. Plasmas* **18** 123503
[7] Dordizadeh P, Adamiak K and Castle G S P 2016 *Plasma Sources Sci. Technol.* **25** 065009
[8] Liu L and Becerra M 2016 *J. Phys. D: Appl. Phys.* **49** 225202
[9] Liu L and Becerra M 2017 *J. Phys. D: Appl. Phys.* **50** 105204
[10] Monrolin N, Praud O and Plouraboué F 2018 *Phys. Plasmas* **25** 063503
[11] Bourdon A, Pasko V P, Liu N Y, Celestin S, Segur P and Marode E 2007 *Plasma Sources Sci. Technol.* **16** 656
[12] Zheleznyak M B, Mnatsakanyan A K and Sizykh S V 1982 *High Temp.* **20** 357
[13] Almeida P G C, Benilov M S and Naidis G V 2002 MOBION—code for evaluation of the mobility and temperature of ions in a weakly ionized gas as functions of reduced electric field and gas temperature
[14] Almeida P G C, Benilov M S and Naidis G V 2002 *J. Phys. D: Appl. Phys.* **35** 1577
[15] Sigmond R S 1984 *J. Appl. Phys.* **56** 1355
[16] Pancheshnyi S 2013 *J. Phys. D: Appl. Phys.* **46** 155201
[17] Hagelaar G J M and Pitchford L C 2005 *Plasma Sources Sci. Technol.* **14** 722
[18] Phelps database www.lxcat.net (retrieved 29 January 2019)
[19] Gallagher J W, Beaty E C, Dutton J and Pitchford L C 1983 *J. Phys. Chem. Ref. Data* **12** 109
[20] Haefliger P, Hösl A and Franck C M 2018 *J. Phys. D: Appl. Phys.* **51** 355201
[21] Hösl A, Haefliger P and Franck C M 2017 *J. Phys. D: Appl. Phys.* **50** 485207
[22] Benilov M S and Naidis G V 2003 *J. Phys. D: Appl. Phys.* **36** 1834
[23] Wen X, Yuan X, Lan L, Long M and Hao L 2016 *IEEE Trans. Plasma Sci.* **44** 3386
[24] Chen X, He W, Du X, Yuan X, Lan L, Wen X and Wan B 2018 *Phys. Plasmas* **25** 063525
[25] Naidis G V 2006 *Plasma Sources Sci. Technol.* **15** 253
[26] Bian X, Wang L, Macalpine J M K, Guan Z, Hui J and Chen Y 2010 *IEEE Trans. Dielectr. Electr. Insul.* **17** 63
[27] Liu N, Dwyer J R and Rassoul H K 2012 *J. Atmos. Sol.—Terr. Phys.* **80** 179
[28] Zebboudj Y and Ikene R 2000 *Eur. Phys. J. AP* **10** 211
[29] Xu M, Tan Z and Li K 2012 *IEEE Trans. Dielectr. Electr. Insul.* **19** 1377
[30] Xu P, Zhang B, Chen S and He J 2016 *Phys. Plasmas* **23** 063511
[31] Foord T R 1953 *Proc. IEE II* 100 585
[32] Robinson M 1967 *IEEE Trans. Power. Appar. Syst.* **86** 185
[33] Waters R T and Stark W B 1975 *J. Phys. D: Appl. Phys.* **8** 416
[34] Isa H, Sonoi Y and Hayashi M 1991 *IEEE T. Electr. Insul.* **26** 291
[35] Takahashi A and Nishijima K 1994 *IEEE Trans. Dielectr. Electr. Insul.* **1** 590
[36] Radmilović-Radjenović M, Radjenović B, Matejćik Š and Klas M 2014 *Plasma Chem. Plasma Process.* **34** 55
[37] Mnatsakanyan A K, Naidis G V and Solozobov Yu M 1986 *High Temp.* **24** 771